

RESEARCH

Open Access



Laboratory exploration of a novel method to protect silicate relics against salt efflorescence by directional induction of water

Qiang Li^{1,2,3}, Ge Gao^{1,2}, Longkang Yang^{1,2}, Xiao Huang^{2*} and Hongjie Luo^{1,2,3*}

Abstract

Salt efflorescence is one of the critical problems for the preservation of immovable silicate relics. Salt efflorescence mainly comes from continuous cycles of crystallization/dissolution or hydration/dehydration of salts in confined pores in silicate relics. Many protocols have been developed in attempts to alleviate possible salt damages with minor success because of endless water and salt feed from underground. In this study, we propose and design a novel technique for salt damage prevention and protection of immovable relics. Materials with higher water-absorbing ability than matrix are applied to control the water and salt migration direction in simulated sand samples. The distribution of moisture content on the surface of sand is followed by hyperspectral imaging. It appears that water and salt molecules will preferentially transport towards positions containing higher water-absorbing material. Both organic and inorganic high water-absorbing materials show effective in controlling the water and salt migration direction, which provides a new approach for the prevention and protection of salt efflorescence in silicate cultural relics.

Keywords Salt efflorescence, Cultural relics, High water-absorbing materials (HWAMs), Hyperspectral imaging

Introduction

Silicate relics are among the most abundant and important cultural relics and historical sites around the world, which are mainly made of silicate minerals. Many of silicate relics are immovable cultural relics [1–6]. They record the traces of human historic activities and are of major value to scientific research and cultural education [7]. However, due to factors such as natural erosion and environmental changes, the current conservation state of

these silicate cultural relics is not optimistic. Salt efflorescence are the most widespread diseases in grottoes, murals and earthen sites, which are directly or indirectly associated with the transport of soluble salts [8–10]. Damages occur when soluble salts are transported to the surface of silicate cultural relics for crystallization by capillary action and diffusion [11]. Two of the most abundant and destructive salts found in silicate cultural relics are sodium sulfate and sodium chloride, and the destructive effects of salt efflorescence are mainly attributed to the stress generated during salt crystallization [12]. If proper actions are not employed timely, soluble salts will continuously migrate upward with groundwater. Coupled with changes in temperature and humidity of the external environment, the salt solution residing in the pores of cultural relics will constantly undergo crystallization-dissolution process, ultimately resulting in the destruction of cultural relics [13–16].

There have been many studies for the prevention and protection of salt efflorescence. Crystallization modifiers

*Correspondence:

Xiao Huang
xhuang@shu.edu.cn
Hongjie Luo
hongjieluo@shu.edu.cn

¹ School of Materials Science and Engineering, Shanghai University, Shanghai 200444, China

² Institute for the Conservation of Cultural Heritage, Shanghai University, Shanghai 200444, China

³ Shanghai Institute of Ceramics, Chinese Academy Sciences, Shanghai 200050, China



© The Author(s) 2024. **Open Access** This article is licensed under a Creative Commons Attribution 4.0 International License, which permits use, sharing, adaptation, distribution and reproduction in any medium or format, as long as you give appropriate credit to the original author(s) and the source, provide a link to the Creative Commons licence, and indicate if changes were made. The images or other third party material in this article are included in the article's Creative Commons licence, unless indicated otherwise in a credit line to the material. If material is not included in the article's Creative Commons licence and your intended use is not permitted by statutory regulation or exceeds the permitted use, you will need to obtain permission directly from the copyright holder. To view a copy of this licence, visit <http://creativecommons.org/licenses/by/4.0/>. The Creative Commons Public Domain Dedication waiver (<http://creativecommons.org/publicdomain/zero/1.0/>) applies to the data made available in this article, unless otherwise stated in a credit line to the data.

(inhibitors or promoters) are one of the approaches, which aims to reduce the crystallization pressure or to promote salt crystallization occurring at the surface rather than in the pores of the cultural relics [17–19]. Ferrocyanide, citrate, organophosphorus compounds and borax are the most studied crystallization modifiers in the field of heritage conservation [20–25]. However, the method is not always feasible and effective. Crystallization modifiers are typically effective only for specific types of salts, and environmental problems associated with modifiers are inconclusive [26, 27]. In addition, the crystallization modifiers will lead to a significant increase in concentration of soluble salts in silicate cultural relics, which arouses serious concerns.

Several studies have shown that blocking the pathway of salt solution migration from the interior of relics to the surface layers, such as constructing a so-called water-salt barrier in between, is an effective solution to control salt efflorescence in heritage [28–31]. Similar technique is currently applied in the prevention of salinization in agricultural land [32, 33]. The principle of the technology is by reducing the suction of the matrix in the soil water transport layer. Generally, the larger the particle size used, the more durable its water-salt barrier effect [34]. This technique has been demonstrated to be effective to some extent, and it has the potential to destroy silicate cultural relics.

It is often observed that salt efflorescence is not homogeneously distributed in immovable heritages. And some positions always show worse or much more obvious salt efflorescence than other positions. Paper pulp can be applied on the salty spots to remove some salt [35]. This is a quite common conservation practice used by many conservators. The inhomogeneous salty distribution seems due to the inhomogeneous water absorbing ability at different spots. Until now, protections against salt efflorescence mainly focus on treating salts. As we all known, soluble salts transport with water. So, if we can control the water absorbing ability of different spot in cultural heritages, can we control the spots where salt efflorescence occurs?

In this work, a novel method and technique for salt efflorescence prevention and protection in silicate cultural relics using high water-absorbing materials (HWAMs) is proposed. It is primarily based on the assumption that the migration and crystallization of salt molecules can be controlled by manipulating water migration. Here two HWAMs, one organic polymer and one inorganic silicate material with significantly different water absorbing ability, are applied. The study examines the effect of two HWAMs on the directional induction of water and salt migration in sand. Additionally, it provides a preliminary evaluation of the

feasibility of this approach for salt efflorescence prevention and protection in silicate cultural relics.

Experimental

Sample preparation

In this work, commercial sand (the average particle size is 150 μm shown in Figure S1) was used as the medium for water-salt transport experiments after it was cleaned with deionized water and dried. Sodium polyacrylates, commercial super absorbent polymers (SAPs) and pottery were employed as organic and inorganic HWAMs, respectively. The pottery sample were designed and fired between the temperature of 900–1050 $^{\circ}\text{C}$, with small aperture, high water absorption and moderate strength, as inorganic superabsorbent materials. The pore size distribution and porosity of pottery is shown in Figure S2. And the pottery and sand samples were ultrasonically cleaned with deionized water until the conductivity of washing water was below 0.055 $\mu\text{S}/\text{cm}$, then were dried in a vacuum oven at 110 $^{\circ}\text{C}$ for 6 h. Sodium chloride solution (0.1 mol/L) was used as salt solution reservoir. A plexiglass box (length 22 cm, width 22 cm and height 21 cm) with a perforated bottom was used as the experimental base.

Experimental setup

The experimental schematic is shown in Figure S3, and the schematic diagram of simplified laboratory experiment is shown in Figure S4. A realistic picture of the relic in actuality is shown in Figure S5.

Sample characterization

The morphology of samples was characterized using a scanning electron microscope (SEM, Mwelin Compact, Carl Zeiss NTS GmbH, German) coupled with energy dispersive spectroscopy (Oxford) at an accelerating voltage of 15 kV. Ion chromatography (Thermo Scientific DIONEX Aquion AQ-1200) was performed to characterize the anion concentration of the samples. Hyperspectral images of quartz sand surface were collected in the short-wave infrared (SWIR) range of 1000–2500 nm with a spectral resolution of 5.6 nm. The system consisted of an InGaAs camera (320 \times 240 pixels; Sensors Unlimited, Inc., Princeton, NJ, USA), a spectrograph (ImSpector N25E, Spectral Imaging Ltd., Oulu, Finland), five halogen lamps (3 \times 50 W and 2 \times 20 W), a One-axis electric stepping mobile platform (IRCP0076-1COMB, Isuzu Optics Corp., Taiwan, China), data acquisition software (Spectral Image software, Isuzu Optics Corp., Taiwan, China).

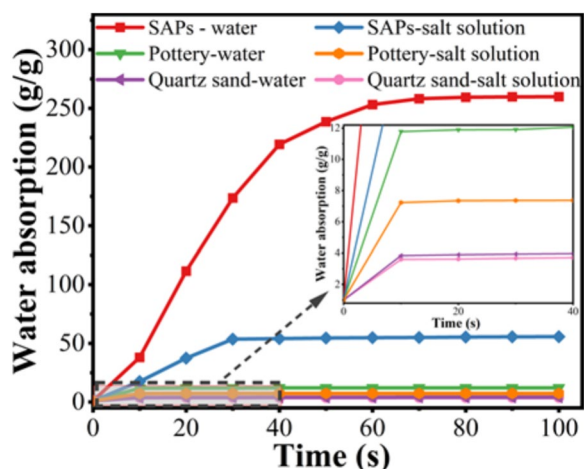


Fig. 1 The water and salt solution absorption curves of quartz sand and HWAMs

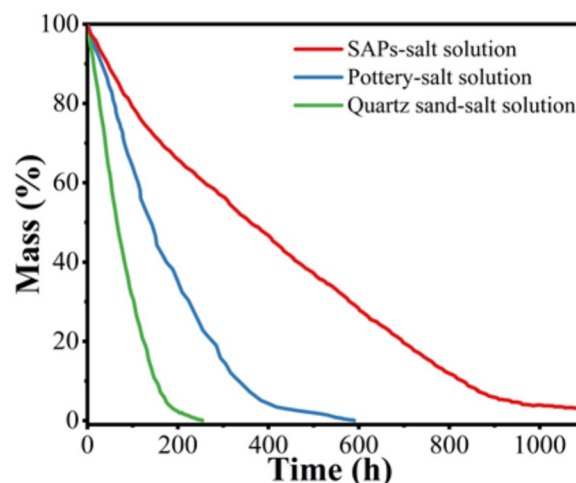


Fig. 2 Water-retention capacity of quartz sand and HWAMs

Result and discussion

Water and salt solution absorption capacity of water absorbent materials

In order to determine the water absorption capacity of two HWAMs, water absorption curves were established for them in pure water and salt solution systems, respectively. It can be seen from Fig. 1 that the water absorption capacity of SAPs was significantly higher than that of pottery and quartz sand. The water absorption rate of SAPs was relatively fast in the first 40 s, and then gradually decreases to reach the water absorption equilibrium. The absorption capacity of SAPs on the salt solution was significantly reduced compared to pure water system, and reached stability after 30 s. It was attributed to the reduced osmotic pressure within and outside the ionic network structure of SAPs. Compared with the pure water system, there were no differences in the absorption of salt solution by pottery and quartz sand, but the salt solution mass was higher than that of pure water due to the same filling volume of salt water and pure water in the pores.

The water-retention capacity of HWAMs is a critical indicator that affects their upper limit of utilization. In order to obtain the water-retention capacity of different water-absorbent materials for salt solution, the weight loss curves of water evaporation at room temperature were measured separately, and the results are shown in Fig. 2. The pottery samples were completed with water evaporation at 600 h. However, the SAPs was not completely evaporated at up to 1000 h. The SAPs has an extremely strong ability to hold water at room temperature, while the pottery samples are easily subject to water evaporation, and the specific surface area is the primary reason for the rate of water dissipation.

Visualization of moisture content in simulated medium surface

Hyperspectral imaging has been found to be effective in predicting moisture content, offering the advantage of non-destructive and visual characterization. Furthermore, this technique has been fully approved in a previous study [36–38]. We used this method to predict the moisture content of sand surfaces. The moisture content distribution on the surface of sand was obtained by providing deionized water from the bottom. The effect of water-absorbing materials in preventing and protecting cultural relics from salt efflorescence was explored by hyperspectral imaging technique. The main step was that the moisture content of each pixel point was inversed out by an image processing program prepared in MATLAB. A calibration model based on the characteristic wavelength is applied to predict the moisture content of each pixel in the image, which is presented as a pseudo-colored. The spectral information of sand with different water content (0–0.45 g/g) was collected by hyperspectral imaging technique, and the raw data were pre-processed by SG smoothing, and the results are shown in Fig. 3.

The successive projection algorithm (SPA) [39, 40] was used to extract the characteristic wavelengths of the raw spectra of SWIR hyperspectral imaging, as shown in Fig. 4a and b. When the maximum characteristic wavelength was selected as 8, the smallest root means square error (RMSE) value of 0.00184 was obtained in SWIR spectra. At this time, the model fitting effect is the best, and 3 characteristic wavelengths were selected. It is evident in Fig. 4c that the support vector regression (SVR) model for moisture content developed by the characteristic wavelengths has a better prediction performance.

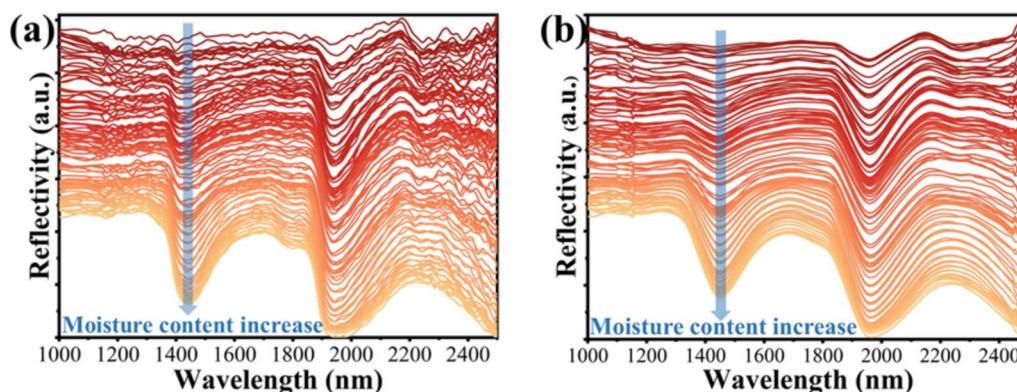


Fig. 3 a Raw spectra b Savitzky-Golag preprocessed spectra of 101 sand samples with different moisture

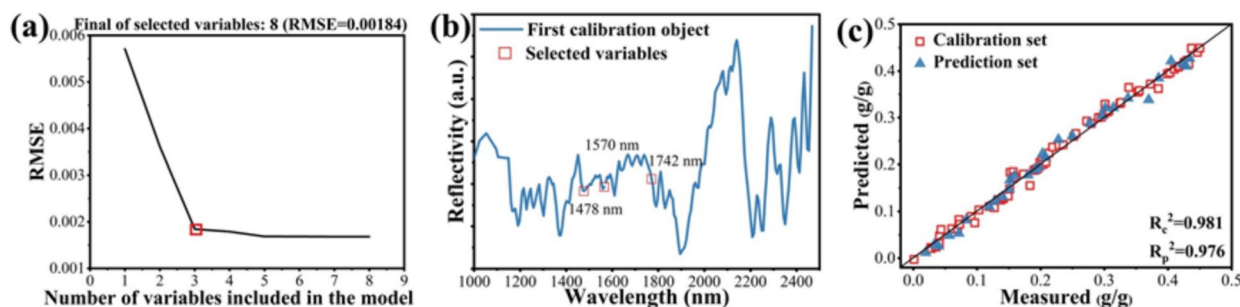


Fig. 4 a, b Characteristic wavelengths extraction of the raw spectra in SWIR by successive projection algorithm (SPA), and c Scatter plots of the measured and predicted moisture content values of sand in support vector regression model

In order to facilitate the realization of moisture content in simulated medium surface, SG-MSC was used to process the original image under characteristic wavelengths (1478 nm, 1570 nm, 1742 nm). Besides, the processed simulated medium surface images were generated by multiplying the model's regression coefficients for each pixel of the image. It can be seen from Fig. 5 that the pixels color of the image with higher moisture content was displayed in red, while the image with lower content was shown in green. To facilitate the analysis of the water content distribution of sand, the black color is employed to indicate the HWAMs. With the increase of moisture content of sand, the color of the image will change to red. Visualizing distribution map of sand offered a more intuitive and comprehensive assessment of moisture content of each pixel, which also has provided a novel approach to silicate cultural relics. The results showed that several water-absorbing materials could induce more water to their nearby locations, reducing the moisture content of distant samples and thus preventing the occurrence of salt efflorescence to silicate cultural relics to some extent. On the contrary, for sample without water-absorbing materials, water was continuously transported from the bottom to the surface over time with diffusion and

capillary action. As shown in Fig. 5a, the moisture content of sand was higher in the boundary at 13 days. At 25 days, the moisture content on the surface of sand was increasing and the distribution had no obvious regularity.

Chloride ion concentration distribution of simulated medium

In order to determine the effect of different absorbent materials on simulated medium for salt efflorescence prevention, seven parallel samples were set up simultaneously. The chloride ion concentration distribution was obtained after equally interval sampling at different days, and the results were shown in Fig. 6. It is clear from the results that the simulated medium without absorbent material has the highest chloride ion concentration on the edge at 3 days due to interfacial effects. And chloride ion concentration shows a disorderly distribution at 25 days.

Figure 7 shows the Cl^- concentration on the surface of the sand protected by the absorbent material. It is concluded that the Cl^- content of the sand not protected with any absorbent material increases dramatically with time, and the ion content is much higher at any time than that of the sand protected by HWAMs. Additionally,

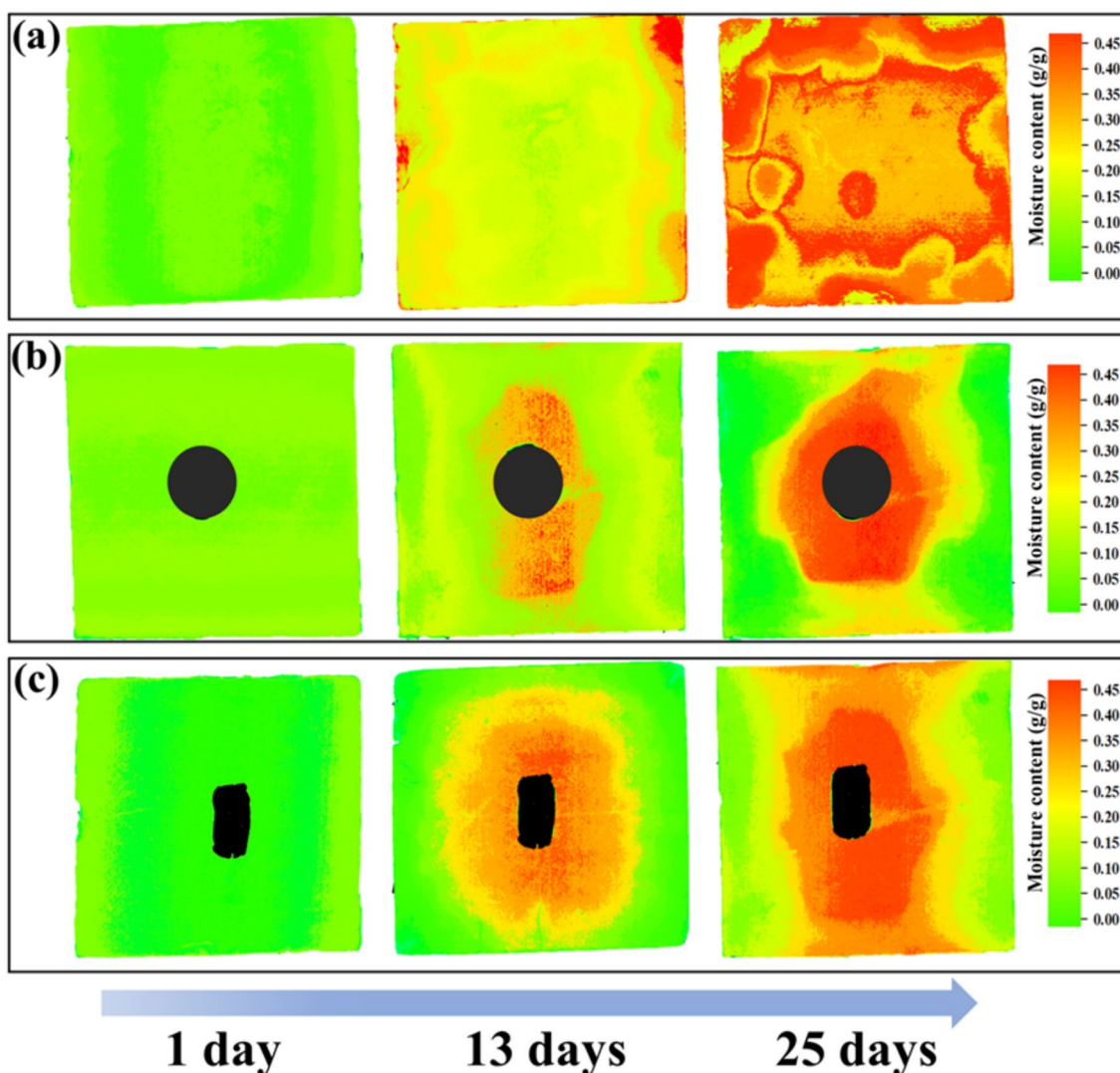


Fig. 5 Two-dimensional distribution maps of moisture content in sand surfaces by hyperspectral imaging: **a** Reference sample, **b** SAPs, **c** pottery

the chloride ion content on the surface of sand is thus the result of the synergistic effect of water retention and absorption (Fig. 8). In particular, due to the strongest water absorption capacity of SAPs, there is virtually no chlorine ion content on the sand in 0–10 days. The water absorption capacity of the pottery was relatively low, and the chloride ion content of the sand was slightly elevated from 0 to 10 days. However, the Cl^- content of sand under SAPs protection increased more rapidly in 13–25 days compared to the pottery. This illustrates that the ability of SAPs to absorb salt solutions is significantly reduced in the late stage of water-salt transport. And its super water retention capacity leads to less water dissipation and cannot form the gradient of liquid content between SAPs and sand again. Therefore, more salt

solution inside was transferred to the surface of sand by capillary and diffusion effects, which caused the Cl^- content to increase dramatically. On the contrary, the relatively inferior water-retention capacity of pottery causes the salt solution inside to be transferred to the surface, where water is dissipated and salt crystals precipitate due to the external environment. This increased the duration of the liquid concentration gradient between pottery and sand, resulting in a relatively slow increase in the Cl^- content of sand. The large specific surface area promotes the evaporation of water and also prompts the salt solution in the foundation to move continuously toward the pottery, and the solution eventually reaches supersaturation crystallization on the surface of the pottery, achieving the purpose of directing the salt to crystallize at the

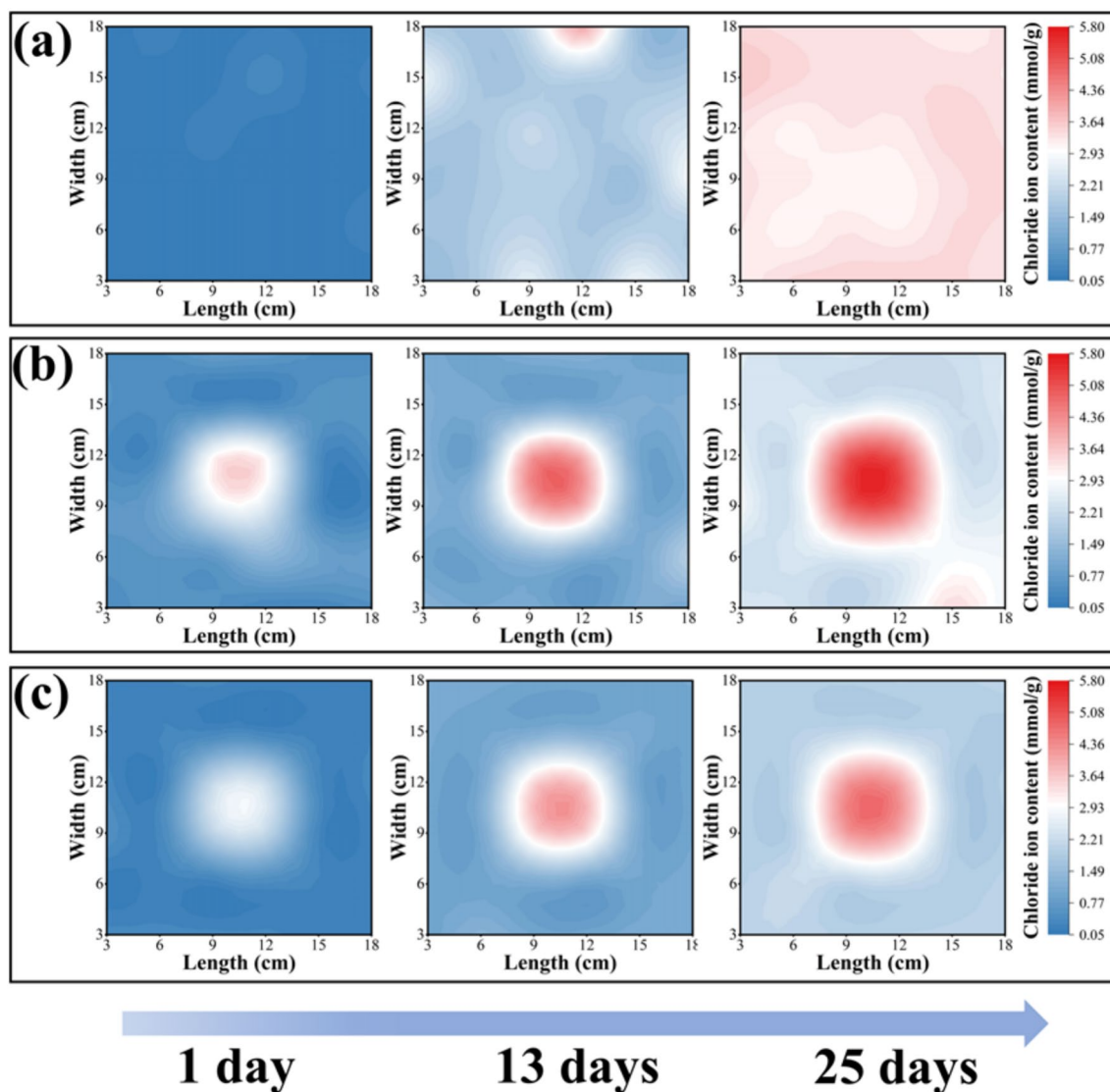


Fig. 6 Chloride ion content distribution on the surface of simulated medium at different days. **a** Reference sample, **b** SAPs, **c** pottery

specified location and preventing the salt efflorescence. Such results can be also observed by naked eyes. In Fig. 9, Fig. 9a and b are side and overhead view of the simulated sample after directional induction of water using pottery. It is obvious all salts migration to pottery and crystallize on pottery surface. On the other hand, salts basically crystallize on the surface of the simulated sample without water conduction treatment as shown in Fig. 9c.

In order to explain intuitively the effect of water-absorbing materials on the salt content of sand, the average Cl^- concentration at equally interval depths in sand profiles were shown in Fig. 8, and the average Cl^- concentration distribution was shown in Fig. 10. The solution at the bottom migrates through the pores to the surface

and connects to the atmosphere, causing the salt solution concentration to reach supersaturation as the water is continuously evaporated, resulting in the formation of salt crystals. The absorbent material was inserted into the sand to a depth of 6 cm, and there was no variation in salt solution concentration at depths of sand under 6 cm. The average chloride ion concentration at a depth of 2 cm in the sand profile without any HWAMs increased dramatically with time and salt crystals almost covered the surface of the sand at 21 days. And the Cl^- content in the surface sand surpassing 3.0 (mmol/g) by day 25. In contrast, there was a gradual increase in Cl^- content in the surface sand of the experimental group using SAPs, did not exceed 2.5 (mmol/g) until day 25. But the chloride

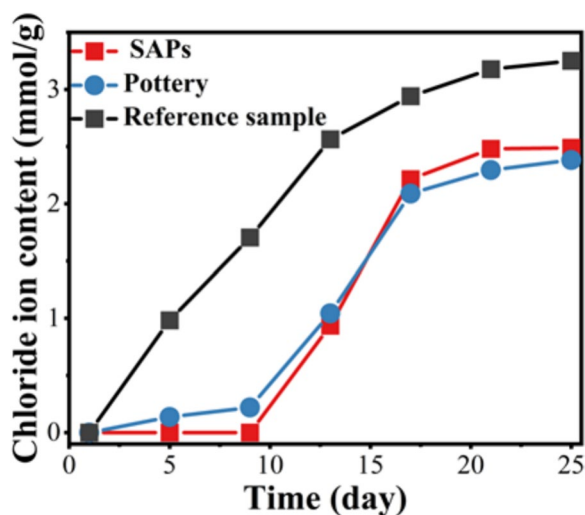


Fig. 7 Average Cl⁻ content on the surface of sand at different days

ion concentration of sand protected by water-absorbing materials increases more gradually, which is due to more salt solution being adsorbed into the internal pores of water-absorbing materials. In particular, the Cl⁻ concentration of sand under the action of SAPs increased marginally after 13 days. This is a sufficient indication that the presence of salt is a significant impediment to the water absorption performance of SAPs. In the initial stage, the SAPs have a reticulate loose porous structure, which makes it possible for the solution to enter the pores easily by capillary action and diffusion. When SAPs absorbed the salt solution, the salt ions affected its reticular structure and the polymer chains contracted under the shielding effect of counter ions, resulting in a sharp decrease in the water absorption capacity of SAPs. The results demonstrate the superior effect of SAPs inducing solution migration before reaching the water absorption limitation. However, the pottery samples were able to

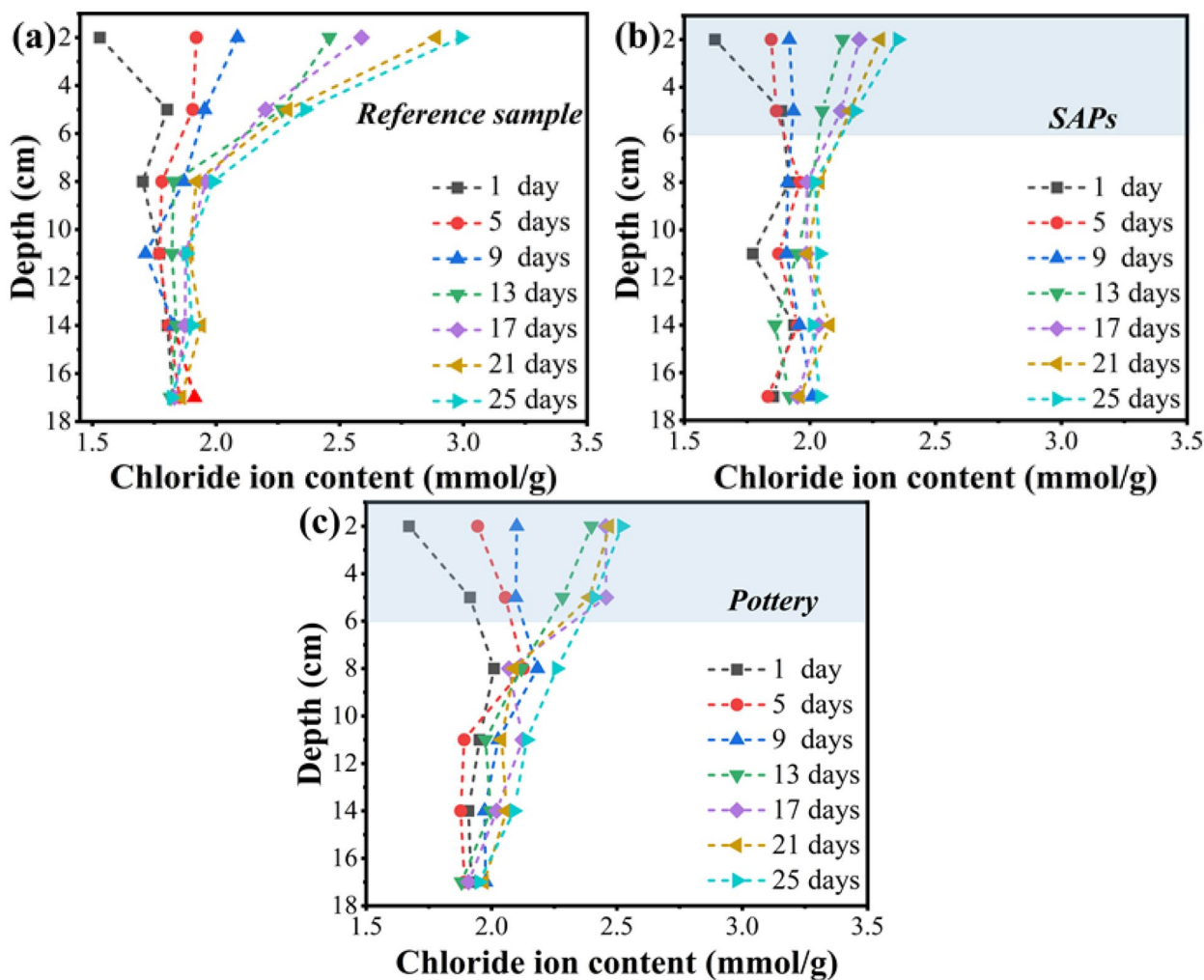


Fig. 8 The average content of Cl⁻ in the sand profile at 1 day, 5 days, 9 days, 13 days, 17 days, 21 days, 25 days of the four groups: a reference sample, b SAPs, c pottery

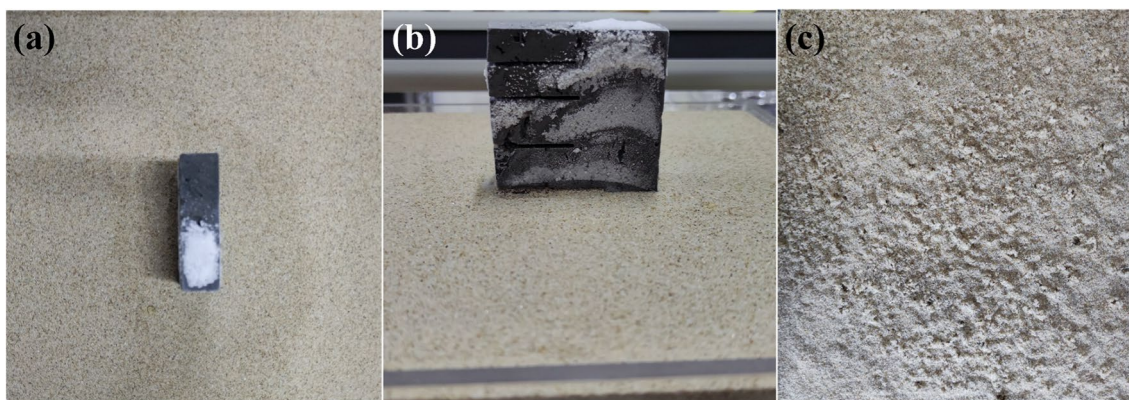


Fig. 9 Photographs of **a** side view; **b** overhead view of the simulated sample after directional induction of water using pottery; white solids are salts **c** overhead view of control sample; salt is basically precipitated on the surface

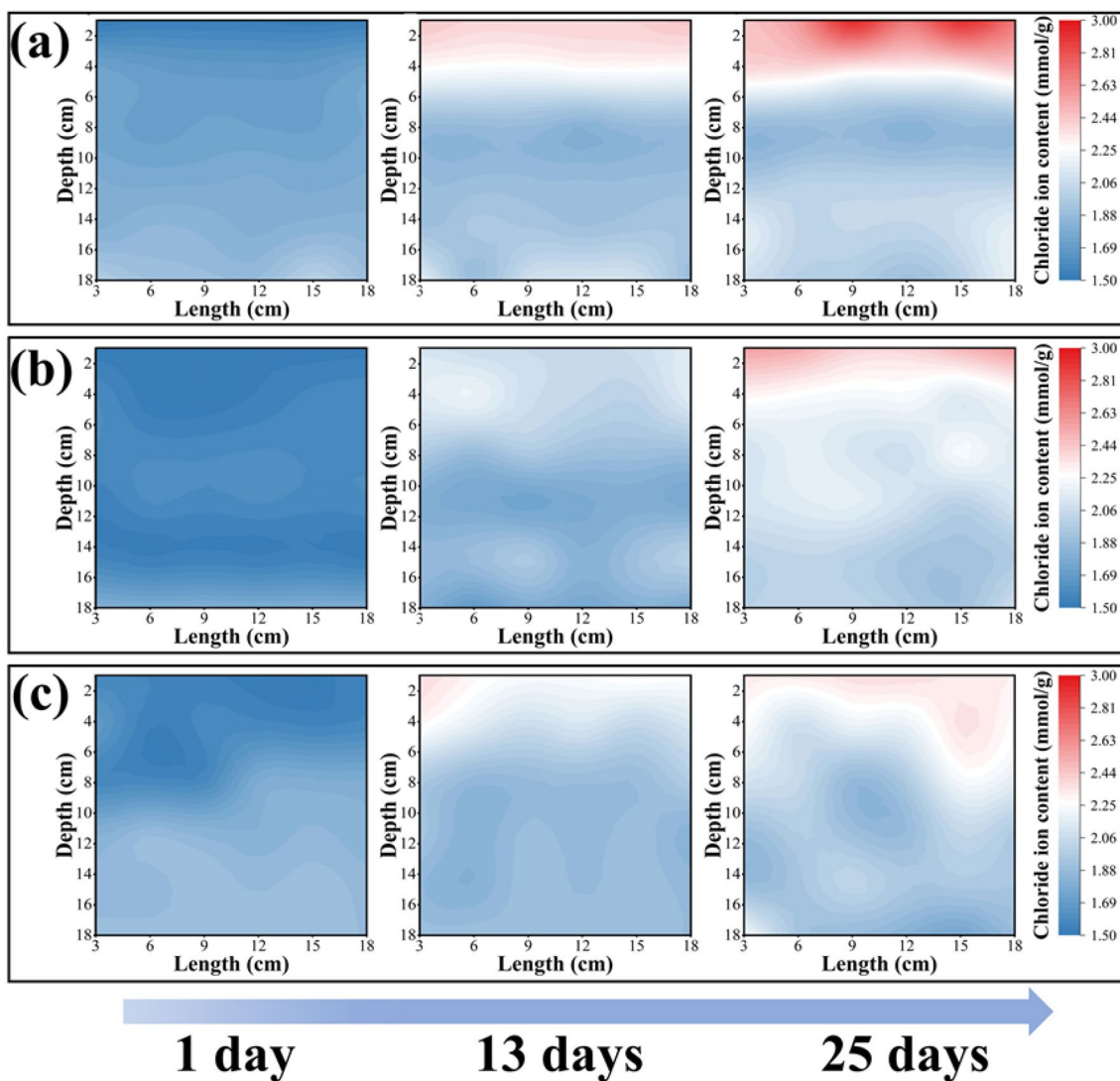


Fig. 10 The content of Cl^- distribution in the sand profile at different days. **a** Reference sample, **b** SAPs, **c** pottery

induce migration for a long time, more importantly, the pottery can be re-used in this situation after rinsing with deionized water. Direct observation with naked eyes and SEM images (see Figure S6 in supporting information) show there are no observable changes of the pottery after absorbing salt and water rinse.

Conclusion

This research explores the possibility of inducing water directional migration for application in salt efflorescence prevention and protection of cultural relics. The induction of water-salt transport by two water-absorbing materials is investigated, and the feasibility of different HWAMs in salt efflorescence prevention of cultural relics is verified. Based on the optimal water content prediction model of sand, the water content distribution can be obtained by hyperspectral imaging, which demonstrates visually the directional migration of water under the effect of HWAMs. Organic HWAMs used in this work is extremely effective in inducing directional migration of salt solutions before reaching the limit of its water absorption, however, once the water absorption reaches saturation, it loses its water-inducing effect.

The water absorbing ability of inorganic HWAMs used is much weaker than its organic partner. But it is still efficient in inducing salt solution migration. Meanwhile, it has the advantage of long-term effectiveness after regular salt removal from the surface, and can be used repeatedly. In summary, our results show that directional induction of water and salt migration in silicate cultural relics can be realized by using HWAMs, and the method developed in this work is effective in controlling the salt migration. The protocol proposed in this work provides a novel approach for the prevention and protection of salt efflorescence in silicate cultural relics. But more research work is needed for field applications in the future.

Supplementary Information

The online version contains supplementary material available at <https://doi.org/10.1186/s40494-024-01271-9>.

Supplementary Material 1.

Acknowledgements

The authors are grateful to the financial supports from the National Key Research and Development Project of China (No. 2019YFC1520104, 2020YFC1521804), Key Program of National Natural Science Foundation of China (No. 51732008). This study is also supported by the grant (Protection and Research of Important Paleontological Fossil Resources of Chongqing) from the Chongqing Municipal Planning and Natural Resources Bureau.

Author contributions

LQ: conducted most of the experiments and data analyses, wrote the initial draft of this manuscript; GG and YLK: implemented the viscosity and sublimation experiments and data analyses; LQ and XH: conceptualized the research, interpreted data and finalized the manuscript; HLJ: helped to design the experiment setup, revised the manuscript. All authors read and approved the final manuscript.

Availability of data and materials

All data analyzed during this study are included in this published article. Raw data are available upon request.

Declarations

Ethics approval and consent to participate

Not applicable. This manuscript does not report data generation or analysis.

Competing interests

The authors declare that they have no known competing financial interests or personal relationships that could have appeared to influence the work reported in this paper.

Received: 22 December 2023 Accepted: 3 May 2024

Published online: 14 May 2024

References

1. Qu J, Cao S, Li G, et al. Conservation of natural and cultural heritage in Dunhuang, China. *Gondwana Res.* 2014;26:1216–21.
2. Lu KA, Zi A, Niu RA, et al. Using surface nuclear magnetic resonance and spontaneous potential to investigate the source of water seepage in the JinDeng Temple grottoes, China. *J Cult Herit.* 2020;45:142–51.
3. Ortiz R, Ortiz P, Colao F, et al. Laser spectroscopy and imaging applications for the study of cultural heritage murals. *Constr Build Mater.* 2015;98:35–43.
4. Richards J, Viles H, Guo Q. The importance of wind as a driver of earthen heritage deterioration in dryland environments. *Geomorphology.* 2020;369:107363.
5. Pei QQ, Wang XD, Zhao LY, et al. A sticky rice paste preparation method for reinforcing earthen heritage sites. *J Cult Herit.* 2020;44:98–109.
6. Xu QM, Zhou HN, Huang X, et al. In-situ formation of one-dimensional silica for conservation of silicate relics using cellulose nanocrystals as templates. *J Cult Herit.* 2023;62:349–55.
7. Hui Z, Qiang L, Liu T, et al. The preservation damage of hydrophobic polymer coating materials in conservation of stone relics. *Prog Org Coat.* 2013;76:1127–34.
8. Zhang C, Zhang B, Cui B. High hydrophobic preservation materials can cause damage to Tabia relics. *Prog Org Coat.* 2020;145:105683.
9. Zhang L, Zhang J, Guo Q, et al. Quantitative assessment of weathering of cretaceous sandstone relics in Longdong Area from the surface to the interior. *Sediment Geol.* 2022;441:106265.
10. Xia B, Xz A, Wei T, et al. The negative impact of skylights on light-irresponsible historical sites within archaeological museums: a case study. *Sol Energy.* 2020;202:104–14.
11. Han W, Gong R, Liu Y, et al. Influence mechanism of salt erosion on the earthen heritage site wall in Pianguan Bastion. *Case Stud Constr Mater.* 2022;17: e01388.
12. Han W, Pei S, Liu F. Material characterization of the brick in the Ming Dynasty heritage wall of Pianguan County: a case study. *Case Stud Constr Mater.* 2022;16: e00940.
13. Granneman S, Lubelli B, Hees R. Effect of mixed in crystallization modifiers on the resistance of lime mortar against NaCl and Na₂SO₄ crystallization. *Constr Build Mater.* 2019;194:62–70.
14. D'Agostino D, Macchia A, Cataldo R, et al. Microclimate and salt crystallization in the crypt of Lecce's Duomo. *Int J Archit Herit.* 2015;9:290–9.
15. Nikhil KD, Rathish KP. Investigations on alternate lime-pozzolana based mortars for repair of heritage structures. *Constr Build Mater.* 2022;341:127776.

16. D'Altri AM, Miranda SD, Beck K, et al. Towards a more effective and reliable salt crystallisation test for porous building materials: predictive modelling of sodium chloride salt distribution. *Constr Build Mater*. 2021;304:124436.
17. Ribeiro APB, Masuchi MH, Miyasaki EK, et al. Crystallization modifiers in lipid systems. *J Food Sci Technol*. 2015;52:3925–46.
18. Rivas T, Alvarez E, Mosquera MJ, et al. Crystallization modifiers applied in granite desalination: the role of the stone pore structure. *Constr Build Mater*. 2010;24:766–76.
19. Facchinetto SE, Tanize B, Neumann GE, et al. Synthesis of submicrometer calcium carbonate particles from inorganic salts using linear polymers as crystallization modifiers. *J Braz Chem Soc*. 2017;28:547–56.
20. Lubelli B, Hees R. Effectiveness of crystallization inhibitors in preventing salt damage in building materials. *J Cult Herit*. 2007;8:223–34.
21. Ergen D, Feijoo J, Fort R, et al. Effects of potassium ferrocyanide used for desalination on lime composite performances in different curing regimes. *Constr Build Mater*. 2020;259:120409.
22. Flatt RJ, Mohamed NA, Caruso F, et al. Predicting salt damage in practice: a theoretical insight into laboratory tests. *RILEM Tech Lett*. 2017;2:108–18.
23. Franceschini M, Broggi A, Santarelli ML, et al. Effectiveness of phosphocitrate as salt crystallization inhibitor in porous materials: case study of the roman mosaic of orpheus and the beasts (Perugia, Italy). *Int J Archit Herit*. 2015;9:195.
24. Ruiz-Agudo E, Putnis CV, Pel L, et al. Template-assisted crystallization of sulfates onto calcite: implications for the prevention of salt damage. *Cryst Growth Des*. 2013;13:40–51.
25. Granneman SJ, Lubelli B, van Hees RP. Characterization of lime mortar additivated with crystallization modifiers. *Int J Archit Herit*. 2018;12:5.
26. Granneman SJ, Lubelli B, van Hees RP. Mitigating salt damage in building materials by the use of crystallization modifiers—a review and outlook. *J Cult Herit*. 2019;40:183–94.
27. Saleh MM, Darwish SS, Elzoghby M. The effectiveness of some crystallization inhibitors in preventing salt damage to limestone. *J Cryst Growth*. 2022;585:126606.
28. Yang Y, Chu J, Xiao Y, et al. Seepage control in sand using bioslurry. *Constr Build Mater*. 2019;212:342–9.
29. Chen Y, Gao Y, Ng CW. A new capillary barrier system for retaining wall backfilled with fine-grained soil. *Comput Geotech*. 2020;118:103324.1–103324.8.
30. Munns R. Physiological processes limiting plant growth in saline soils: some dogmas and hypotheses. *Plant Cell Environ*. 2010;16:15–24.
31. Zhao W, Cao T, Dou P, et al. Effect of various concentrations of superabsorbent polymers on soil particle-size distribution and evaporation with sand mulching. *Sci Rep*. 2019;9:3511.
32. Li X, Zhang C. Effect of natural and artificial afforestation reclamation on soil properties and vegetation in coastal saline silt soils. *CATENA*. 2020;198:105066.
33. Xie Z, Wang Y, Cheng G, et al. Particle-size effects on soil temperature, evaporation, water use efficiency and watermelon yield in fields mulched with gravel and sand in semi-arid Loess Plateau of northwest China. *Agric Water Manage*. 2010;97:917–23.
34. Chang B, Wen H, Yu CW, et al. Preservation of earthen relic sites against salt damages by using a sand layer. *Indoor Built Environ*. 2022;31:1142–56.
35. Pel L, Sawdy A, Voronina V. Physical principles and efficiency of salt extraction by poulticing. *J Cult Herit*. 2010;11:59–67.
36. Wei Y, Wu F, Xu J, Sha J, Zhao Z, He Y, Li X. Visual detection of the moisture content of tea leaves with hyperspectral imaging technology. *J Food Eng*. 2019;248:89–96.
37. Wang Z, Fan S, Wu J, Zhang C, Xu F, Yang X, Li J. Application of long-wave near infrared hyperspectral imaging for determination of moisture content of single maize seed. *Spectrochim Acta A*. 2019;248:89–96.
38. Xuan G, Gao C, Shao Y, Wang X, Wang Y, Wang K. Maturity determination at harvest and spatial assessment of moisture content in okra using Vis-NIR hyperspectral imaging. *Postharvest Biol Technol*. 2021;180:111597.
39. Gao G, Li Q, Hao P, Huang X, Luo H. Luminescent properties of $Mg_{1.99}SnO_4:0.01Mn^{2+}$ phosphors doped with Zn^{2+} . *J Materiomics*. 2023;9:510–5.
40. Gao G, Li Q, Luo H, Huang X. Preparation and performance evaluation of humidity-sensitive color-changing materials via hyperspectral imaging. *Sens Actuator A-Phys*. 2023;362:114660.

Publisher's Note

Springer Nature remains neutral with regard to jurisdictional claims in published maps and institutional affiliations.